ACS APPLIED ENERGY MATERIALS

www.acsaem.org Article

Investigations Into Aqueous Redox Flow Batteries Based on Ferrocene Bisulfonate

Zhiling Zhao, Baosen Zhang, Briana R. Schrage, Christopher J. Ziegler,* and Aliaksei Boika*

Cite This: *ACS Appl. Energy Mater.* 2020, 3, 10270–10277 Read Online

ACCESS | Metrics & More | Article Recommendations | Supporting Information

ABSTRACT: The successful implementation of redox flow battery (RFB) technology requires the development of highly stable and soluble catholyte and anolyte materials that could be used in aqueous media. In this work, we investigated a highly soluble derivative of ferrocene—1,1′-bis(sulfonate)-ferrocene dianion disodium salt—as a possible catholyte in an all-anionic RFB design. Based on the results of cyclic voltammetry and charge/discharge cycling experiments, we determined that this compound can be unstable and prone to a nucleophilic attack by anions in certain supporting electrolytes. However, it is stable in neutral pH solutions with weak nucleophilic anions like nitrate. These findings are fundamental for the future development of improved RFB materials.

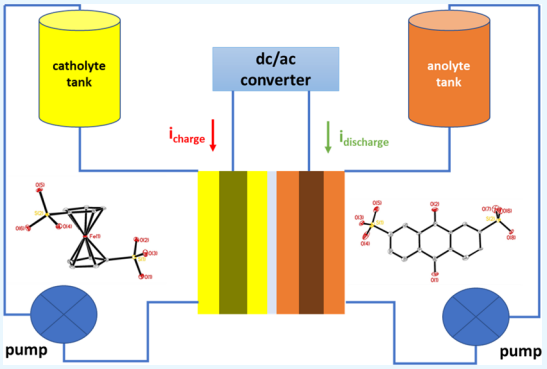

KEYWORDS: *anionic catholyte, water-soluble ferrocene, flow cell, cyclic voltammetry, charge/discharge*

INTRODUCTION

During the past few decades, the development of renewable energy sources has attracted much attention because of their potential to reduce the carbon footprint of electricity generation.[1] However, these sources, such as solar and wind energy, are intermittent and unpredictable; thus, an energy storage technique is required.[2,3] Lithium-ion batteries are good candidates for energy storage because of their outstanding performance.[4] Recently, an alternate technique, the redox flow battery (RFB) has become commercially viable, which not only has low cost but also offers longer lifetimes and improved safety.[2,5,6] The energy and power of an RFB can be decoupled in this technology by controlling the volume of electrolytes and the size of the RFB stack.[7] Thus, RFB devices are advantageous for electrical energy storage and suitable for large-scale applications. RFBs can be classified by the redox species used in the electrolyte solution or the solvent system.[2,8] For the purpose of green energy storage, aqueous RFBs have gained more attention than nonaqueous RFBs. A series of molecular strategies ranging from transition-metal species to organic compounds have been developed as the redox active species for aqueous RFB applications.[9−16] Yet, many of these redox active materials exhibit drawbacks, such as cost and low abundance materials for vanadium RFBs, self-discharging issues because of the crossover of the free ligand (triethanolamine) for all-soluble all-iron RFBs, and corrosive electrolytes for alkaline quinone RFBs.[9,10,13]

Because iron is an earth-abundant element, attention has turned to the redox-active organometallic compound, ferrocene. Because this compound exhibits very reversible oxidation and reduction and its chemistry is well understood, researchers have showed interest in applying ferrocene derivatives to RFB development.[12,17−19] Because of the limited solubility of unmodified ferrocene in water, RFBs using ferrocene initially focused on nonaqueous solvent systems.[17,18] To meet the requirements of green chemistry, the development of aqueous ferrocene-based RFBs with a high working voltage has been initiated and received some success by utilizing the hydrophilic ammonium functional group.[12,19] On account of the positively charged ferrocene units, viologen derivatives have been typically paired as an anolyte.[12,18,19] However, a well-known viologen derivative, *N*,*N*′-dimethyl-4,4′-bipyridinium dichloride (paraquat), is known to be toxic and may lead to significant health problems after long-term exposure.[20,21] RFBs are ideally operated at high concentrations to reach high capacity; thus, large amounts of viologen derivatives present in RFB tanks would present a potential hazard.

To address these problems, we have focused on the development of anionic ferrocenes as highly soluble and reversible redox active materials. In this report, we present aqueous RFB which consists of sulfate-modified ferrocene as

Received: September 14, 2020
Accepted: October 2, 2020
Published: October 15, 2020

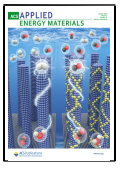

https://dx.doi.org/10.1021/acsaem.0c02259
ACS Appl. Energy Mater. 2020, 3, 10270−10277

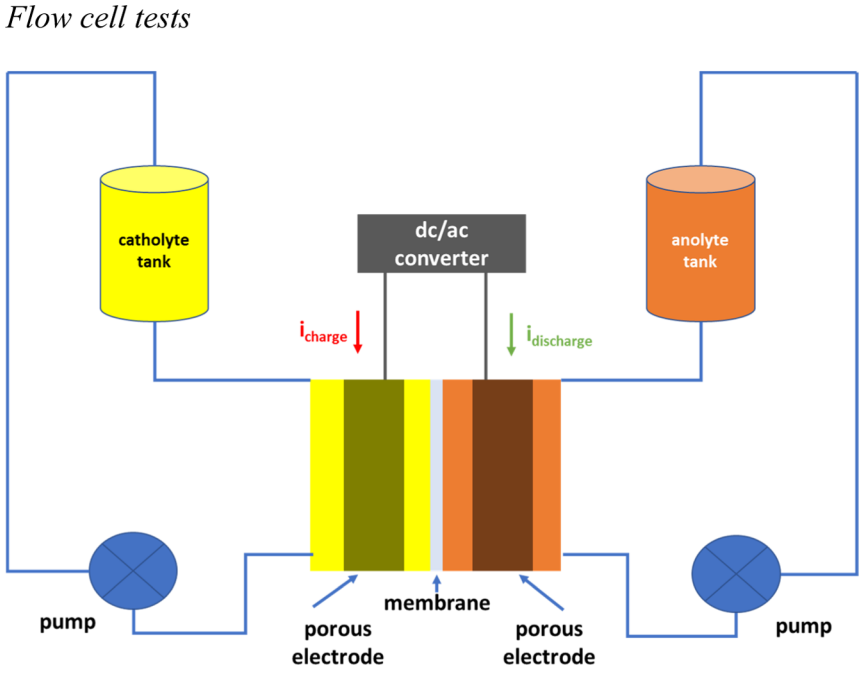

Figure 1. Schematic diagram of an "all-aqueous" RFB.

the catholyte and anthraquinone-2,7-disulfonic acid disodium salt (2,7-AQDS) as the anolyte. Both of these compounds are highly soluble in water due to the presence of the sulfonate functional groups. 1,1′-bis(sulfonate)ferrocene dianion disodium salt (1,1′-FcDS) was found to be oxidized at a more positive potential than (ferrocenylmethyl)trimethylammonium cations because of the higher electron withdrawing strength of the sulfonate functional group.[22] Thus, RFB using 1,1′-FcDS as the catholyte is expected to generate a larger working voltage. Moreover, it opens up the possibility of adopting neutral or negatively charged redox species as the anolyte such as, for example, anthraquinones. Compared to highly toxic paraquat (acute oral LD_{50} 75 mg/kg in rats) used as the anolyte in aqueous ferrocene-based RFB, anthraquinones are much safer, and 2,7-AQDS has an acute oral LD_{50} (in rats) up to 4000 mg/kg.[23,24] Anthraquinones are widely used in food, pharmaceutical, and paper industries, and their application to RFBs has been explored extensively.[11,13,25] To avoid the formation of unstable free radicals during RFB operation, a slightly acidic low-cost acetate buffer and 0.5 M H_2SO_4 were tested, respectively, as a supporting electrolyte in this work.[26] In addition, ethylene glycol (EG) was added to improve the solubility of both 1,1′-FcDS and 2,7-AQDS in aqueous solutions, which was found to increase the solubility of 2,7-AQDS.[25] We observed that the properties and stability of the RFBs were highly dependent on the identity of the supporting electrolyte.

EXPERIMENTAL SECTION

Materials. The catholyte, 1,1′-FcDS, was prepared from bis ferrocene sulfonic acid, which can be synthesized based on a previously reported procedure.[27] Basic iron(III) acetate was generated by a previously published procedure.[28] The anolyte, 2,7-AQDS, was purchased from Pfaltz & Bauer Inc. All other chemicals were of ACS grade and purchased from Sigma-Aldrich or Fisher Scientific and used directly. Nanopure water was obtained from a Milli-Q Integral 5 water purification system (Millipore, Bedford, MA).

X-ray Crystallographic Data Collection and Structure Solution and Refinement. Single-crystal data for all structures were collected on a Bruker CCD-based diffractometer with a dual Cu/Mo ImuS microfocus optics (Cu Kα radiation, λ = 1.54178 Å or Mo Kα radiation, λ = 0.71073). Crystals were mounted on a cryoloop using Paratone oil and placed under a steam of nitrogen at 100 K (Oxford Cryosystems). The data were corrected for absorption with the SADABS program.[29] The structures were refined using the Bruker SHELXTL Software Package (Version 6.1) and solved using direct methods until the final anisotropic full-matrix least squares refinement of F2 converged. electronic supporting information (ESI) available: CCDC 2009128-2009129 contains the supplementary crystallographic data for this paper (Table S1). These data can be obtained free of charge from The Cambridge Crystallographic Data Center via www.ccdc.cam.ac.uk/data_request/cif.

Cyclic Voltammetry Electrochemical Characterization. Electrochemical measurements were conducted using a CHI 920d potentiostat in a standard three-electrode configuration. A platinum wire was used as an auxiliary electrode. The working electrode used in voltammetry experiments was a glassy carbon disk with a diameter of 3 mm. A Ag|AgCl|KCl (2 M) reference electrode was used. The supporting electrolyte was 1 M $NaNO_3$, 2 M acetate buffer (molar ratio between sodium acetate and acetic acid is 1:1, pH 4.53), or 0.5 M H_2SO_4. All solutions were purged with nitrogen or argon prior to any electrochemical measurements.

Cyclic voltammograms (CVs) were collected at scan rates varying from 20 to 65 mV/s for the measurement of the diffusion coefficients (D) of 1,1′-FcDS and 2,7-AQDS using Randles−Sevcik equation. The CVs were compared (at a scan rate of 65 mV/s) for the redox potentials of 1,1′-FcDS and 2,7-AQDS to evaluate the open circuit potential (OCP) under acidic conditions and 1 M $NaNO_3$.

Flow Cell Tests. The flow cell (Figure 1) was constructed using a PEM fuel cell hardware which accepts liquid at both electrodes, two graphite felt electrodes (G100, AvCarb, USA) and a piece of cation exchange membrane (Nafion 117). The surface area of the graphite felt was 9 cm^2. Nafion membrane and graphite felt electrodes were immersed in the supporting electrolyte (1 M $NaNO_3$, 2 M acetate buffer or 0.5 M H_2SO_4) overnight before the charge−discharge tests. Each electrode chamber was connected with an electrolyte reservoir using Versilon 2001 (Saint-Gobain) tubing. Each reservoir contained 30 mL of the 0.03 M catholyte/anolyte and the supporting electrolyte. A Masterflex L/S peristaltic pump (Cole-Parmer, USA) was used to

https://dx.doi.org/10.1021/acsaem.0c02259
ACS Appl. Energy Mater. 2020, 3, 10270−10277

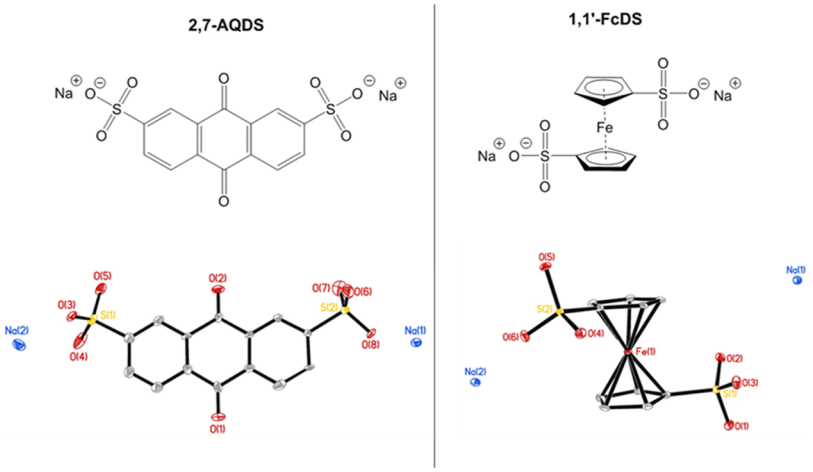

Figure 2. Anolyte (2,7-AQDS): anthraquinone-2,7-disulfonic acid disodium salt (left). Catholyte (1,1′-FcDS):1,1′-bis(sulfonate)ferrocene disodium salt (right). The corresponding crystal structures are shown at the bottom of the diagram with 35% thermal ellipsoids. Hydrogen atoms have been omitted for clarity.

circulate the electrolytes through a flow chamber at a rate of 40 mL/min. Both reservoirs were purged with argon to remove oxygen and then sealed in a glovebox filled with argon before cell cycling. Constant current charge−discharge cycling tests were carried out at 293 K with an Arbin LBT21084 Battery Cycler in a two-electrode configuration. The full cell was charged/discharged at current 25 mA (2.8 mA/cm^2) for 100 cycles.

Solubility Test. The solubility of 1,1′-FcDS in 1 M $NaNO_3$ with and without the addition of EG was measured using UV−visible spectra. Saturated solutions were prepared for both conditions, and supernatant was diluted 100 times (without EG) and 200 times (with EG) for the UV−vis absorbance measurements. The correlation of the peak absorbance (Figure S1C,D) and concentration was calculated using a calibrated relationship of standard samples (Figure S1A,B).

Permeability Test. The permeability of 1,1′-FcDS across the Nafion 117 membrane was evaluated using the flow cell setup. For the solutions in electrolyte reservoirs, one (donating) side was filled with 30 mL of 0.03 M 1,1′-FcDS and 1 M $NaNO_3$, another (receiving) side was filled with 30 mL of 1 M $NaNO_3$. A peristaltic pump was used to circulate the electrolytes at a rate of 40 mL/min for 7 days, during which samples were taken from the receiving side after 24, 120, 144, and 182 h. CVs were collected for the samples so that the concentration of 1,1′-FcDS in each sample could be calculated using the peak current values (by comparing to the CVs of 1,1′-FcDS with a known concentration). The permeability was calculated using the method reported by Kwabi et al.[13]

Synthesis. *Synthesis of 1,1′-FcDS.* Ferrocene bis sulfonic acid (5.0 g, 14.5 mmol) was dissolved in 200 mL of ethanol and a solution of concentrated NaOH was slowly added to the mixture and stirred for 30 min. The resulting yellow precipitate was filtered and air dried to yield a yellow solid. Crystals suitable for X-ray diffraction were obtained by the slow evaporation of a dimethylformamide/water mix.

1,1′-FcDS. Yield: 5.4 g (96%). IR: 1366, 1163 cm^{-1} (ν_{SO}). ^{1}H NMR (300 MHz, DMSO-d_6): 4.12 (s, 4H on C_5H_4), 4.33 (s, 4H on C_5H_4). ^{13}C{^{1}H} NMR (125 MHz, DMSO-d_6): δ = 96.9, 69.7, 68.5. HRMS (ESI-TOF, negative mode) m/z: calcd for $C_{10}H_8FeNaO_6S_2$, 366.9015; found, 366.9060 [M − Na]$^-$.

RESULTS AND DISCUSSION

Ferrocene derivatives have been widely utilized in materials chemistry.[30] Most of the ferrocene compounds have good solubilities in organic solvents but not in water. Therefore, previously they have often been applied in nonaqueous RFB systems.[17,18] Over the past several years, aqueous ferrocene-based RFB systems have been explored using ferrocene ammonium compounds, producing all-cationic RFBs employing anion exchange resins.[12] We have explored the synthesis of new ferrocene-based electroactive materials and have recently presented work on all-ferrocene salts where large potential differences are observed between the anolyte and catholyte.[27] Unfortunately, those all-ferrocene salts are not practical for RFBs that use ion exchange resins, as either the ferrocene anion or ferrocene cation bind to the oppositely charged ion-exchange resin, thus impeding function.

For the work presented here, we employed a water-soluble ferrocene compound functionalized with SO_3^- groups, 1,1′-FcDS (Figure 2). This compound can be readily prepared from commercially available reagents and exhibits high solubility in water.[27] Along with this species, we also employed the bis sulfonate-modified anthraquinone 2,7-AQDS, which also exhibits good water solubility and is commercially available. Thus, this is an all-anionic approach to the RFB problem, using sulfonates as stable functional groups to drive optimal aqueous solubility. Sulfonate modification is frequently used in drug design to impart water solubility, and this functional group can also be readily applied to the RFB problem.

The synthesis of 1,1′-FcDS is accomplished via the sulfonation of ferrocene, followed by neutralization of the bis-sulfonic acid derivative to afford the sodium salt. We were able to structurally characterize 1,1′-FcDS, along with the 2,7-AQDS salt, using single-crystal X-ray methods. The structures are shown in Figure 2 below their chemical diagrams. As can be seen in the structures, each compound exhibits two peripheral sulfonate groups. The presence of these anionic functional groups is key to transforming the hydrophobic precursors into highly water-soluble compounds.

We determined the solubility of 1,1′-FcDS in various solvents using UV−vis measurements, and the results are shown in Table 1 as well as Figure S1. In 1 M $NaNO_3$, the solubility is 0.3 M and theoretical capacity is 8 Ah/L [assuming 0.3 M 1,1′-FcDS as a catholyte; theoretical capacity = solubility (M) × 96,485 (C/mol)/3,600 (C/Ah)]. Previously, it was reported that the addition of EG enhanced the solubility of 2,7-AQDS because of the interactions between the polar and nonpolar groups of EG and 2,7-AQDS.[25] Therefore, we expected that EG could also increase the solubility of 1,1′-FcDS because it has both a polar (sulfonyl) group and nonpolar (phenyl) group. We found that by adding 0.5 M EG

https://dx.doi.org/10.1021/acsaem.0c02259
ACS Appl. Energy Mater. 2020, 3, 10270−10277

Table 1. Solubility and Capacity Data of 1,1′-FcDS and 2,7-AQDS

compound (supporting electrolyte)	solubility (M)	capacity (Ah/L)
1,1′-FcDS (1 M $NaNO_3$)	0.3	8.0
1,1′-FcDS (1 M $NaNO_3$, 0.5 M EG)	0.6	16.1
2,7-AQDS (1 M KCl)[a]	0.3	16.1
2,7-AQDS (1 M KCl, 0.5 M EG)[a]	0.8	42.9

[a]From ref 25.

in 1 M $NaNO_3$ solution, the solubility of 1,1′-FcDS increases to 0.6 M. In addition, the theoretical RFB capacity reaches 16.1 Ah/L.

Electrochemical Properties. CVs were collected to characterize the electrochemical properties of 1,1′-FcDS and 2,7-AQDS. When the compounds were dissolved in 1 M $NaNO_3$, 1,1′-FcDS showed a half-wave potential, $E_{1/2}$, equal to 0.65 V, and 2,7-AQDS showed an $E_{1/2}$ = −0.45 V (Figure 3). Therefore, based on these results, an OCP for the RFB composed of 1,1′-FcDS as a catholyte and 2,7-AQDS as an anolyte is expected to be *ca.* 1.1 V.

We further analyzed the CV data to determine the diffusion coefficients of the redox species. Using the Randles−Sevcik equation, the diffusion coefficient of 1,1′-FcDS was calculated to be 1.46 × 10^{-6} cm^2/s (without EG). With EG added, the diffusion coefficient of 1,1′-FcDS decreased to 1.29 × 10^{-6} cm^2/s (based on the CVs in Figure S8), presumably because of the higher viscosity for EG (0.0161 Pa·s for pure EG) versus water (0.0009 Pa·s). The obtained diffusion coefficient in water was comparable with the value published for (ferrocenylmethyl)trimethylammonium in aqueous RFB.[12] The electrochemical data for 1,1′-FcDS are summarized in Table 2. The electrochemical behavior of 2,7-AQDS was also evaluated here under the same conditions for 1,1′-FcDS (Table 2). Apart from the neutral pH supporting electrolyte, 1 M $NaNO_3$, CVs were also collected in acidic supporting electrolyte solutions: 2 M acetate buffer (pH 4.53) and 0.5 M H_2SO_4 (Figures S9 and S10).

It is known that anthraquinone derivatives (AQ) can form a radical anion during electrochemical reduction in neutral and alkaline electrolytes (eq 1)[26]

$$AQ + AQ^{2-} \leftrightarrow 2AQ^{-} \quad (1)$$

To avoid the degradation of 2,7-AQDS during reduction, acidic supporting electrolytes were adapted and compared to the behavior in 1 M $NaNO_3$. The $E_{1/2}$ of 2,7-AQDS shifts from −0.458 V in 1 M $NaNO_3$ to −0.234 V in 2 M acetate buffer.

Table 2. Estimated Electrochemical Data for 1,1′-FcDS and 2,7-AQDS

compound (supporting electrolyte)	$E_{1/2}$ (V) versus (Ag|AgCl)	D (cm^2/s)
1,1′-FcDS (1 M $NaNO_3$)	0.652	1.46 × 10^{-6}
1,1′-FcDS (1 M $NaNO_3$, 0.5 M EG)	0.651	1.29 × 10^{-6}
1,1′-FcDS (2 M acetate buffer)	0.642	3.90 × 10^{-7}
1,1′-FcDS (0.5 M H_2SO_4)	0.628	2.09 × 10^{-6}
2,7-AQDS (1 M $NaNO_3$)	−0.458	5.13 × 10^{-7}
2,7-AQDS (2 M acetate buffer)	−0.234	4.18 × 10^{-7}
2,7-AQDS (0.5 M H_2SO_4)	−0.025	3.38 × 10^{-8}

This trend is consistent with the finding that AQ's reduction potential is pH dependent.[26] According to the $E_{1/2}$ values, a 0.9−1.1 V OCP is expected for the 1,1′-FcDS/2,7-AQDS RFB at various pH conditions.

Flow Cell Tests under Different pH Conditions. The 1,1′-FcDS/2,7-AQDS RFB performance at neutral pH, 1 M $NaNO_3$ was evaluated first. The 100-time cycling was performed at 25 mA (Figure S11), and the initial ten charge/discharge cycles are shown in Figure 4A. The trends of the coulombic efficiency (CE), voltage efficiency (VE), and energy efficiency (EE) of the 1,1′-FcDS/2,7-AQDS RFB are shown in the Figure 4C. The EE stays at 60% and the CE is stable above 99%. However, a large loss in capacity (from 0.008 to 0.002 Ah) is observed (Figure 4B). Presumably, the degradation of the capacity results from 2,7-AQDS, which partially decomposes under the basic/neutral conditions.[26]

To eliminate the formation of the AQ^- radical, an acidic supporting electrolyte using acetate buffer was tested for the flow cell operation. Acetate buffer can also maintain the pH 4.53 of the electrolyte during charge/discharge processes. A concentration of 2 M was chosen to match the ionic strength of the buffer to 1 M $NaNO_3$. The initial ten charge/discharge cycles are shown in Figure S13A, while 100 cycles are included in Figure S12. From the charge/discharge data, the cell voltage decreases to ∼0.5 V. This working voltage is much lower than expected; an OCP of ∼0.9 V is expected if calculated using $E_{1/2}$, as listed in Table 2. A possible reason is the formation of a new species during the charge/discharge process, due to the decomposition of 1,1′-FcDS; this is discussed at the end of the Results and Discussions section. The first supporting evidence is the decrease of the diffusion coefficient (D) for 1,1′-FcDS in acetate buffer (Table 2). There is no report in the literature showing an increase in viscosity of acetate buffer solutions; therefore, the viscosity change from 1 M $NaNO_3$ to 2 M

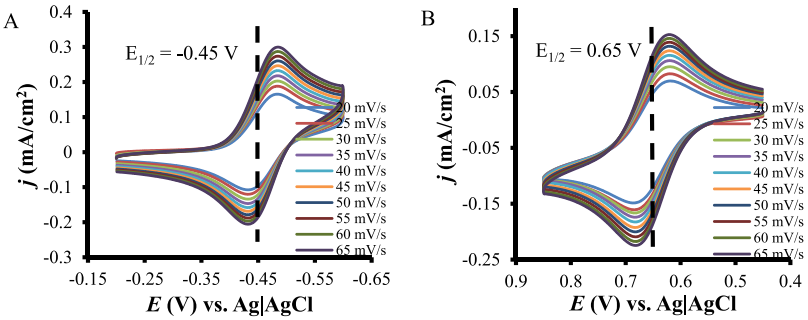

Figure 3. CVs of 2 mM 2,7-AQDS (A) or 2 mM 1,1′-FcDS (B) in aqueous solution containing 1 M $NaNO_3$ as a supporting electrolyte. Working electrode: 3 mm dia. Glassy carbon, reference electrode: Ag|AgCl|KCl (2 M), counter electrode: platinum wire. From the inner curve to outer one, the scan rate varies from 20 to 65 mV/s.

https://dx.doi.org/10.1021/acsaem.0c02259
ACS Appl. Energy Mater. 2020, 3, 10270−10277

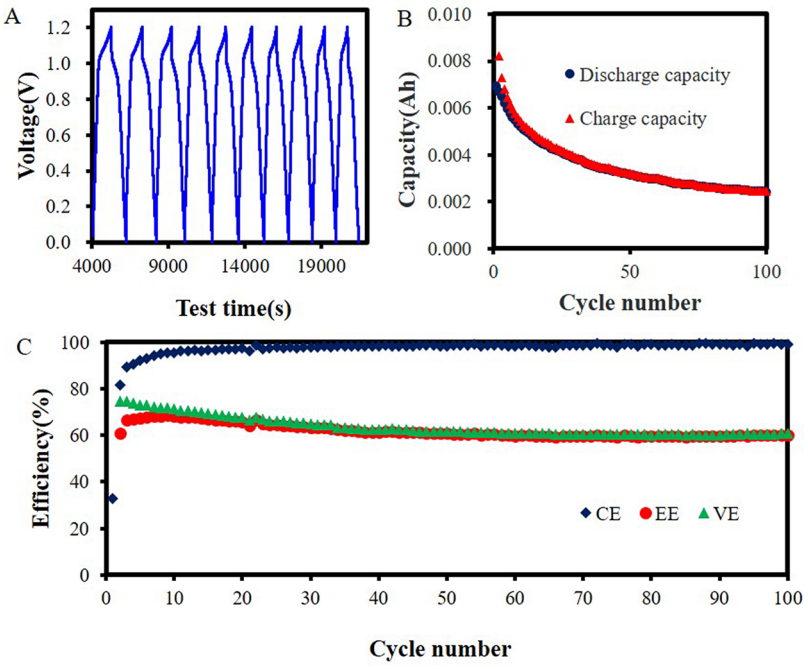

Figure 4. 1,1′-FcDS/2,7-AQDS RFB using 1 M $NaNO_3$ as the supporting electrolyte (0.5 M EG added). (A) Ten charge and discharge cycles (#2 to #11 cycles) at constant current 25 mA (2.8 mA/cm^2); (B) capacity versus cycle number; and (C) CE, EE and VE vs cycle number.

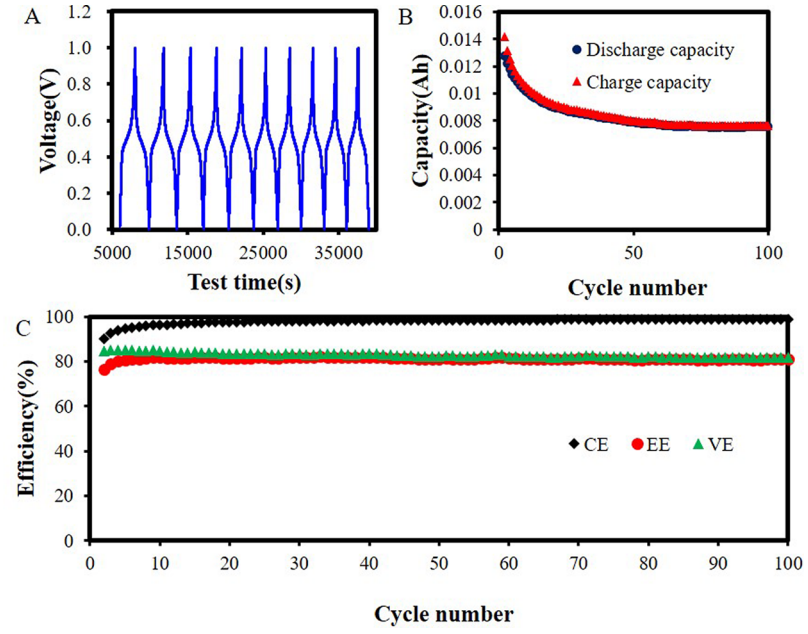

Figure 5. 1,1′-FcDS/2,7-AQDS RFB using 0.5 M H_2SO_4 as a supporting electrolyte. (A) Ten charge and discharge cycles (#2 to #11 cycles) at constant current 25 mA (2.8 mA/cm^2); (B) capacity versus cycling number; and (C) CE, EE, and VE vs cycling number.

acetate buffer should be negligible. Thus, the change of *D* is probably an indication for the irreversible electrochemical process involving 1,1′-FcDS and the formation of a new species, iron(III) acetate (discussed below). It has been reported that electrochemical oxidation product Fc^+ can undergo a nucleophilic attack and destroy the Fe redox centers.[31] With those unusual behaviors observed in the acetate buffer, EE decreased by 10% compared to the RFB using 1 M $NaNO_3$ (Figure S13C). In terms of capacity, the decay under the basic/neutral condition was not observed; it is stabilized around 0.0075 Ah (Figure S13B). It seems the acidic environment created by the acetate buffer improves the capacity by stabilizing the 2,7-AQDS. However, the potential interaction of acetate ions with 1,1′-FcDS may lead to additional problems such as the mentioned formation of iron(III) acetate.

Sulfuric acid as a supporting electrolyte was utilized in the flow-cell test as well. The initial ten charge/discharge cycles are shown in Figure 5A. CE, VE, and EE versus cycle number are shown in Figure 5C. The CE is stable above 99%. This indicates that the cross-over rate of 1,1′-FcDS and 2,7-AQDS is very low. For the negatively charged 1,1′-FcDS and 2,7-

https://dx.doi.org/10.1021/acsaem.0c02259
ACS Appl. Energy Mater. 2020, 3, 10270−10277

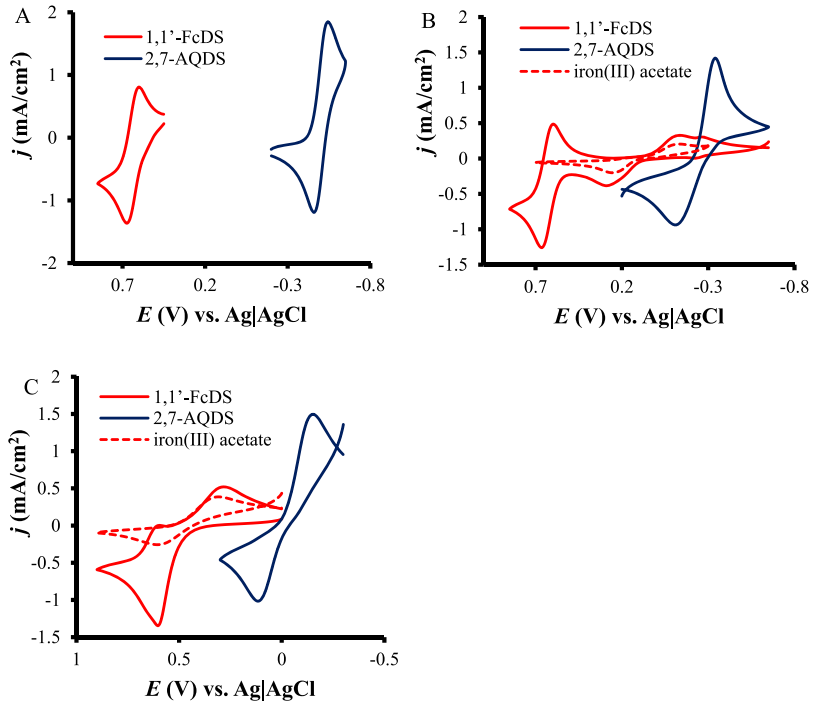

Figure 6. CVs of the catholyte (1,1′-FcDS) and anolyte (2,7-AQDS) after 100 cycles of charge/discharge. (A) Using 1 M $NaNO_3$ as a supporting electrolyte, scan rate: 30 mV/s; (B) using 2 M acetate buffer as a supporting electrolyte, dashed curve: CVs of iron(III) acetate in 2 M acetate buffer, scan rate: 30 mV/s; and (C) using 0.5 M H_2SO_4 as supporting electrolyte, dashed curve: CVs of iron(III) sulfate in 0.5 M H_2SO_4, scan rate: 25 mV/s. In all experiments, working electrode: 3 mm dia. Glassy carbon, reference electrode: Ag|AgCl|KCl (2 M), counter electrode: platinum wire.

AQDS, when redox reactions take place, it is difficult to penetrate a Nafion membrane, which is a cation-exchange membrane. This leads to a low cross-over rate and high CE. However, the cell voltage of the RFB is sacrificed because low pH causes reduction potential of 2,7-AQDS shift to a higher value (Table 2). Yet, EE stays at 80%, which is a high EE value for a ferrocene-based aqueous RFB. The decay of capacity (Figure 5B) is observed during the first 20 cycles and capacity stays around 0.008 Ah thereafter. This capacity fading situation is improved compared to the flow cell under basic/neutral conditions (Figure 4B). Thus, the acidic environment stabilizes the active species during the charge/discharge electrochemical reactions and avoids the severe decrease of the RFB capacity.

Decomposition of the Electrolyte during Cell Cycling. In order to determine what chemical process is taking place in the RFB cell in the cycling experiments, we first characterized the 1,1′-FcDS solution in acetate buffer after a typical series of 100 charge/discharge cycles. We isolated a red crystalline material which we determined was basic iron(III) acetate. This compound has a highly stable trimeric cluster structure comprised six peripheral bridging acetate units binding the triiron core and a central μ-oxo atom.[32] The cluster is monocationic and quite stable in aqueous solution. Additionally, we investigated the UV−visible spectra of the solutions of 1,1′-FcDS in acetate buffer and in H_2SO_4 upon completion of the cell cycling process. The spectra revealed mixtures of 1,1′-FcDS and either iron acetate or Fe(III) ions for the acetate buffer and H_2SO_4 conditions, respectively (see Supporting Information, Figures S6 and S7).

We also recorded a series of CVs for the catholyte and anolyte species after the 100 charge/discharge cycles had been completed; the results are shown in Figure 6. While the data in neutral 1 M $NaNO_3$ (Figure 6A) did not show the presence of a new redox species, under acidic conditions the CVs indicated the transformation of the catholyte as indicated by the appearance of additional peaks at more negative potentials (Figure 6B,C). Because in the acetate buffer electrolyte the formation of iron(III) acetate had been confirmed by X-ray crystallography, we decided to record a CV for this compound and compared it to the CV for the catholyte solution after the cycling. The comparison of peak potentials confirmed a good agreement, as shown in Figure 6B. This fact further confirms our initial argument regarding the decomposition of 1,1′-FcDS because of the nucleophilic attack by the acetate ions. Interestingly, we were also able to confirm the nature of the additional peaks for the catholyte, as shown in Figure 6C (0.5 M H_2SO_4). Based on the results, as shown in Figure 6B, we suspected that the nucleophilic attack by the sulfate ions could be responsible for the decomposition of the catholyte; a recorded CV for iron(III) sulfate confirmed this (dashed line in Figure 6C).

Solution Cross-over Rate Measurements. To investigate the performance of used the Nafion117 membrane and the reason for large capacity fade for our RFB systems, we surveyed the membrane by characterizing the permeability of 1,1′-FcDS (see Experimental Section for the details of the procedure). The membrane shows excellent performance with a low permeability of 1.67×10^{-9} cm^2/s (Figure S15), which is lower than the permeability of the Nafion117 membrane for vanadium ions.[3333] These results confirm that the cross-over of 1,1′-FcDS is not the main reason for large capacity loss.

■ CONCLUSIONS

Ferrocene-based catholyte materials are gaining increased popularity; however, little is done to understand the

https://dx.doi.org/10.1021/acsaem.0c02259
ACS Appl. Energy Mater. 2020, 3, 10270−10277

fundamentals of their operation under various conditions. This paper investigates the behavior of one of such materials, 1,1′-FcDS for potential RFB applications under neutral and acidic conditions. The derivative of anthraquinone, 2,7-AQDS served as the anolyte in all cases. Both compounds are highly soluble because of their ionic nature, leading to the potential fabrication of a device with high energy density. Additionally, these materials are aqueous soluble, which from a green chemistry perspective which is more preferable than organic media.

The choice of all-anionic catholyte and anolyte was deemed advantageous in that it would eliminate adsorption of the redox species onto a cation-exchange Nafion membrane. Basic electrochemical characterization (cyclic voltammetry) was performed in three environments: neutral (1 M $NaNO_3$) and acidic (2 M acetate buffer pH 4.53 and 0.5 M H_2SO_4) conditions, as well as with addition of EG, and the solubilities of the catholyte and anolyte were measured.

By recording charge−discharge curves in neutral solutions containing EG, we observed substantial capacity fading, which we attributed to irreversible electrochemical behavior on the anolyte side (formation of a radical anion). Trying to remedy this issue, we performed the flow experiments in 2 M acetate buffer solution (pH 4.53). To our surprise, we still observed the decrease in capacity, but now the reason was in the catholyte. Even though ferrocene derivatives are widely regarded as highly reversible electrochemical systems, they are prone to chemical transformations in RFB applications, in this case, to a nucleophilic attack by acetate and sulfate ions, while stable in the presence of nitrate. These findings are fundamental to the development of RFB materials, and our future work will address the uncovered instability of ferrocene derivatives, as well as finding alternative anolyte candidates.

■ ASSOCIATED CONTENT

Supporting Information

The Supporting Information is available free of charge at https://pubs.acs.org/doi/10.1021/acsaem.0c02259.

CVs of 1,1′-FcDS in aqueous solutions with 0.5 M EG, CVs of 2,7-AQDS, charge/discharge cycles for 1,1′-FcDS/2,7-AQDS RFB in 1 M $NaNO_3$, 2 M acetate buffer (pH 4.53), acetate buffer with 0.5 M EG and in 0.5 M H_2SO_4, and X-ray crystal data and structure parameters for 1,1′-FcDS and 2,7-AQDS compounds (PDF)

■ AUTHOR INFORMATION

Corresponding Authors

Christopher J. Ziegler − *Department of Chemistry, The University of Akron, Akron, Ohio 44325, United States;* orcid.org/0000-0002-0142-5161; Email: ziegler@uakron.edu

Aliaksei Boika − *Department of Chemistry, The University of Akron, Akron, Ohio 44325, United States;* orcid.org/0000-0001-8249-0741; Email: aboika@uakron.edu

Authors

Zhiling Zhao − *Department of Chemistry, The University of Akron, Akron, Ohio 44325, United States*

Baosen Zhang − *Department of Chemistry, The University of Akron, Akron, Ohio 44325, United States*

Briana R. Schrage − *Department of Chemistry, The University of Akron, Akron, Ohio 44325, United States*

Complete contact information is available at: https://pubs.acs.org/10.1021/acsaem.0c02259

Author Contributions

The manuscript was written through contributions of all the authors. All the authors have given approval to the final version of the manuscript.

Notes

The authors declare no competing financial interest.

■ ACKNOWLEDGMENTS

The authors are grateful to The University of Akron and the National Science Foundation (CHE-1665267) for support of this research.

■ REFERENCES

(1) Boyle, G. *Renewable Energy*, Boyle, G., Ed.; Oxford Univ. Press. ISBN-10 0199261784. ISBN-13 9780199261789, 2004; p 456.

(2) Wang, W.; Luo, Q.; Li, B.; Wei, X.; Li, L.; Yang, Z. Recent Progress in Redox Flow Battery Research and Development. *Adv. Funct. Mater.* **2013**, *23*, 970−986.

(3) Skyllas-Kazacos, M.; Chakrabarti, M. H.; Hajimolana, S. A.; Mjalli, F. S.; Saleem, M. Progress in Flow Battery Research and Development. *J. Electrochem. Soc.* **2011**, *158*, R55−R79.

(4) Marom, R.; Amalraj, S. F.; Leifer, N.; Jacob, D.; Aurbach, D. A Review of Advanced and Practical Lithium Battery Materials. *J. Mater. Chem.* **2011**, *21*, 9938−9954.

(5) Parasuraman, A.; Lim, T. M.; Menictas, C.; Skyllas-Kazacos, M. Review of Material Research and Development for Vanadium Redox Flow Battery Applications. *Electrochim. Acta* **2013**, *101*, 27−40.

(6) Leung, P.; Li, X.; Ponce de León, C.; Berlouis, L.; Low, C. T. J.; Walsh, F. C. Progress in Redox Flow Batteries, Remaining Challenges and Their Applications in Energy Storage. *RSC Adv.* **2012**, *2*, 10125−10156.

(7) Perry, M. L.; Weber, A. Z. Advanced Redox-Flow Batteries: A Perspective. *J. Electrochem. Soc.* **2016**, *163*, A5064−A5067.

(8) Liu, W.; Lu, W.; Zhang, H.; Li, X. Aqueous Flow Batteries: Research and Development. *Chem.—Eur. J.* **2019**, *25*, 1649−1664.

(9) Skyllas-Kazacos, M.; Grossmith, F. Efficient Vanadium Redox Flow Cell. *J. Electrochem. Soc.* **1987**, *134*, 2950−2953.

(10) Gong, K.; Xu, F.; Grunewald, J. B.; Ma, X.; Zhao, Y.; Gu, S.; Yan, Y. All-Soluble All-Iron Aqueous Redox-Flow Battery. *ACS Energy Lett.* **2016**, *1*, 89−93.

(11) Lin, K.; Chen, Q.; Gerhardt, M. R.; Tong, L.; Kim, S. B.; Eisenach, L.; Valle, A. W.; Hardee, D.; Gordon, R. G.; Aziz, M. J.; Marshak, M. P. Alkaline Quinone Flow Battery. *Science* **2015**, *349*, 1529−1532.

(12) Hu, B.; DeBruler, C.; Rhodes, Z.; Liu, T. L. Long-Cycling Aqueous Organic Redox Flow Battery (AORFB) toward Sustainable and Safe Energy Storage. *J. Am. Chem. Soc.* **2017**, *139*, 1207−1214.

(13) Kwabi, D. G.; Lin, K.; Ji, Y.; Kerr, E. F.; Goulet, M.-A.; De Porcellinis, D.; Tabor, D. P.; Pollack, D. A.; Aspuru-Guzik, A.; Gordon, R. G.; Aziz, M. J. Alkaline Quinone Flow Battery with Long Lifetime at PH 12. *Joule* **2018**, *2*, 1894−1906.

(14) Yan, W.; Wang, C.; Tian, J.; Zhu, G.; Ma, L.; Wang, Y.; Chen, R.; Hu, Y.; Wang, L.; Chen, T.; Ma, J.; Jin, Z. All-Polymer Particulate Slurry Batteries. *Nat. Commun.* **2019**, *10*, 1−11.

(15) Wang, C.; Li, X.; Yu, B.; Wang, Y.; Yang, Z.; Wang, H.; Lin, H.; Ma, J.; Li, G.; Jin, Z. Molecular Design of Fused-Ring Phenazine Derivatives for Long-Cycling Alkaline Redox Flow Batteries. *ACS Energy Lett.* **2020**, *5*, 411−417.

(16) Wang, C.; Yang, Z.; Wang, Y.; Zhao, P.; Yan, W.; Zhu, G.; Ma, L.; Yu, B.; Wang, L.; Li, G.; Liu, J.; Jin, Z. High-Performance Alkaline

Organic Redox Flow Batteries Based on 2-Hydroxy-3-Carboxy-1,4-Naphthoquinone. *ACS Energy Lett.* **2018**, *3*, 2404−2409.
(17) Hwang, B.; Park, M.-S.; Kim, K. Ferrocene and Cobaltocene Derivatives for Non-Aqueous Redox Flow Batteries. *ChemSusChem* **2015**, *8*, 310−314.
(18) Montoto, E. C.; Nagarjuna, G.; Moore, J. S.; Rodríguez-López, J. Redox Active Polymers for Non-Aqueous Redox Flow Batteries: Validation of the Size-Exclusion Approach. *J. Electrochem. Soc.* **2017**, *164*, A1688−A1694.
(19) Beh, E. S.; De Porcellinis, D.; Gracia, R. L.; Xia, K. T.; Gordon, R. G.; Aziz, M. J. A Neutral PH Aqueous Organic−Organometallic Redox Flow Battery with Extremely High Capacity Retention. *ACS Energy Lett.* **2017**, *2*, 639−644.
(20) Bus, J. S.; Gibson, J. E. Paraquat: Model for Oxidant-Initiated Toxicity. *Environ. Health Perspect.* **1984**, *55*, 37−46.
(21) Tanner, C. M.; Kamel, F.; Ross, G. W.; Hoppin, J. A.; Goldman, S. M.; Korell, M.; Marras, C.; Bhudhikanok, G. S.; Kasten, M.; Chade, A. R.; Comyns, K.; Richards, M. B.; Meng, C.; Priestley, B.; Fernandez, H. H.; Cambi, F.; Umbach, D. M.; Blair, A.; Sandler, D. P.; Langston, J. W. Rotenone, Paraquat, and Parkinson's Disease. *Environ. Health Perspect.* **2011**, *119*, 866−872.
(22) Schrage, B. R.; Zhao, Z.; Ziegler, C. J.; Boika, A. Cation-Anion Redox Switching in an All-Ferrocene Salt. *ChemElectroChem* **2018**, *5*, 3624−3627.
(23) Melchiorri, D.; Reiter, R. J.; Sewerynek, E.; Hara, M.; Chen, L.; Nisticò, G. Paraquat Toxicity and Oxidative Damage: Reduction by Melatonin. *Biochem. Pharmacol.* **1996**, *51*, 1095−1099.
(24) Montoya, S. C. N.; Agnese, A. M.; Pérez, C.; Tiraboschi, I. N.; Cabrera, J. L. Pharmacological and Toxicological Activity of Heterophyllaea Pustulata Anthraquinone Extracts. *Phytomedicine* **2003**, *10*, 569−574.
(25) Lee, W.; Permatasari, A.; Kwon, B. W.; Kwon, Y. Performance Evaluation of Aqueous Organic Redox Flow Battery Using Anthraquinone-2,7-Disulfonic Acid Disodium Salt and Potassium Iodide Redox Couple. *Chem. Eng. J.* **2019**, *358*, 1438−1445.
(26) Kelsall, G. H.; Thompson, I. Redox Chemistry of H 2 S Oxidation by the British Gas Stretford Process Part III: Electrochemical Behaviour of Anthraquinone 2, 7 Disulphonate in Alkaline Electrolytes. *J. Appl. Electrochem.* **1993**, *23*, 296−307.
(27) Schrage, B. R.; Zhao, Z.; Boika, A.; Ziegler, C. J. Evaluating Ferrocene Ions and All-Ferrocene Salts for Electrochemical Applications. *J. Organomet. Chem.* **2019**, *897*, 23−31.
(28) Liu, J.; Bo, X.; Li, M.; Yin, D.; Guo, L. Contrastive Study on Porphyrinic Iron Metal-Organic Framework Supported on Various Carbon Matrices as Efficient Electrocatalysts. *J. Colloid Interface Sci.* **2018**, *513*, 438−447.
(29) Sheldrick, G. M. Short History of SHELX. *Acta Crystallogr., Sect. A: Found. Crystallogr.* **2008**, *64*, 112−122.
(30) Astruc, D. Why Is Ferrocene so Exceptional? *Eur. J. Inorg. Chem.* **2017**, *2017*, 6−29.
(31) Cuartero, M.; Acres, R. G.; Bradley, J.; Jarolimova, Z.; Wang, L.; Bakker, E.; Crespo, G. A.; De Marco, R. Electrochemical Mechanism of Ferrocene-Based Redox Molecules in Thin Film Membrane Electrodes. *Electrochim. Acta* **2017**, *238*, 357−367.
(32) Sato, T.; Ambe, F.; Endo, K.; Katada, M.; Maeda, H.; Nakamoto, T.; Sano, H. Mixed-Valence States of [Fe3O-(CH2XCO2)6(H2O)3]·nH2O (X = H, Cl, and Br) Characterized by X-Ray Crystallography and 57Fe-Moessbauer Spectroscopy. *J. Am. Chem. Soc.* **1996**, *118*, 3450−3458.
(33) Shirasaki, K.; Yamamura, T. Direct Observation of Vanadium Ion Permeation Behavior through Nafion 117 Using 48V Radiotracer for All-Vanadium Redox Flow Battery. *J. Membr. Sci.* **2019**, *592*, 117367.

https://dx.doi.org/10.1021/acsaem.0c02259
ACS Appl. Energy Mater. 2020, 3, 10270−10277